High throughput micro-CT scanning of small fossils: preparation, packing, parameters and post-processing

Christy A. Hipsley[1,2], Rocio Aguilar[1,2,3], Jay R. Black[4], Scott A. Hocknull[1,5]

[1]School of BioSciences, University of Melbourne, Parkville, VIC, 3010, Australia.

[2]Museums Victoria, GPO Box 666, Melbourne, VIC, 3001, Australia.

[3]School of Biological Sciences, Monash University, Clayton, Victoria, Australia.

[4] School of Earth Sciences, University of Melbourne, Melbourne, Victoria, Australia.

[5]Queensland Museum, Geosciences, 122 Gerler Rd. Hendra, Queensland, 4011, Australia.

Corresponding author:
Christy A. Hipsley
University of Melbourne
BioSciences 4, Building 147
Parkville, VIC 3010
Australia
christy.hipsley@unimelb.edu.au

Running title: High throughput microCT scanning of small fossils

Abstract

1. High-resolution X-ray computed tomography, or microCT (µCT), enables the collection of three-dimensional phenotypic data from whole objects. The power of µCT to visualise internal features without disarticulation makes it particularly valuable for the study of museum collections, which house huge numbers of small specimens that document the spatio-temporal patterns of life. Despite its potential for systematic analyses, most comparative studies employ only few µCT models, due to the challenges associated with scanning multiple specimens within a project scope.

2. Here we describe a new method for high-throughput µCT scanning of dozens of small (< 2 cm) fossils in a single container, while maintaining nanometre-scale resolution and low consumable costs. Simple objects like pharmaceutical capsules and paper drinking straws are used to safely secure specimens inside a plastic tube on the instrument stage, allowing accurate tracking and digital labelling of individuals in the 3D volume. We also explore the effects of various packing materials and multiple specimens per capsule to minimize reconstruction artefacts caused by sample movement that can degrade image quality and hence µCT investment.

3. We illustrate this method using vertebrate fossils from Queensland Museum, Australia, as part of an ongoing effort to track community responses to climate change over evolutionary time. To stabilise specimens during image acquisition, each fossil was wrapped in archival tissue and placed inside a clear two-piece capsule with its label, making it suitable for long-term storage. Following this system, we optimize the quantity of samples per tube to over 70 fossils, generating high quality 3D models for over 1,000 mammal, frog, and lizard specimens. We provide step-by-step instructions on specimen packing, labelling and µCT scanning, with suggestions on how they can be modified to suit user needs.

4. The proposed method offers a simple and cost-effective technique for collecting consistent, high quality µCT data from hundreds of small specimens with minimal time, handling, and error. This system can be easily amended for other types of wet and dry material such as geological, botanical, and zoological samples, providing greater access to large-scale phenotypic data and contributing new information on the biodiversity of our planet.

Keywords

X-ray computed tomography, microCT, CT scan, 3D data, fossils, geometric morphometrics, high throughput

Introduction

High-resolution X-ray computed tomography, also known as HRXCT or micro-CT (μCT), is an increasingly powerful tool for the non-destructive investigation of whole objects. Functioning like a microscope with X-ray vision, μCT generates high fidelity 3D models of solid material from which the outer layers can be virtually dissected or removed, revealing the inner structure. Starting with multiple radiographs of an object taken over 360°, a computer algorithm is used to digitally convert a stack of 2D X-ray projections, or tomograms, into a 3D volume. Whereas in human medicine the X-ray source rotates around the patient (e.g., computerized axial tomography, or CAT scan), in μCT the object is fixed on a rotating stage while the X-ray tube remains stationary. The differential properties of the object's matter, including thickness and atomic number, interact with the X-ray's energy beam to determine the number of photons that pass through it to reach the detector on the other side. This decrease in electromagnetic radiation, termed X-ray attenuation, results in detector pixels with grayscale values proportional to the radiopacity of the material, meaning that dense regions such as bone or rock appear white or light gray (radiopaque), while muscle or skin appears dark (radiolucent). The massively improved resolution of μCT over standard imaging techniques achieves a detail detectability down to 200 nm (0.2 micrometre) – less than the length of a single bacterium.

Since publication of the first X-ray microtomographic figures nearly four decades ago (Sato et al. 1981; Elliot & Dover, 1982, 1985), μCT has had profound impacts across scientific disciplines. Studies in biomedicine, zoology, geology and paleontology now regularly incorporate μCT imaging, and software for the quantitative analysis of volumetric data are constantly developing (e.g., Fiji [Schlindelin et al., 2012], Blob3D [Ketcham, 2005], Dragonfly [Object Research Systems (ORS) Inc, Montreal, Canada]). Within the biological sciences, μCT has been particularly valuable for the study of museum collections, which contain millions of small, delicate and unique specimens not amenable to traditional (often destructive and/or irreversible) preparation. Worldwide, these collections span taxonomic, geographic and temporal distributions, providing a wealth of information for understanding the past, present and future of biodiversity (Page et al., 2015). Creation of cybertypes, or virtual models of type material, is another emerging application of μCT technology (Faulwetter et al., 2013; Akkari et al., 2018), allowing researchers around the world to interact with voucher specimens. When combined with analyses like geometric morphometrics (GM), these models can be used to test taxonomic hypotheses that could shorten the lagtime between species discovery and formal description (Fontaine et al., 2012; Faulwetter et al., 2014), thus expanding the taxonomic bottleneck.

Despite the increasing use of μCT in systematic biology (Hipsley & Sherratt, 2019), a major challenge remains in the practical imaging of high numbers of specimens within a project scope, for example in the context of large-scale analyses of phenotypic variation. This has proven difficult because of the need for specimens to remain motionless during scan time (minutes to hours), and because each individual must be digitally labelled to match the original specimen's identity and hence retain important information, e.g., material type, locality, stratigraphic age. These issues have so far limited community-level μCT analyses,

which could provide important insights into evolutionary responses to environmental change in small, rare, and/or fossilized taxa.

While some GM studies have included hundreds of (Sherratt et al., 2016; Watanabe et al., 2019) or over a thousand (Simon et al., 2016; Sherratt et al., 2017; Chira et al., 2018; Percival et al., 2019) 3D models, their digital images are often aggregated using different sources (museums, repositories, laboratories), methods (surface scanning, μCT), and parameters (X-ray energy, voxel size, number of projections), making it difficult to integrate and compare findings. For smaller specimens in particular, variation in spatial resolution can result in significant measurement errors, for example in estimated volumes or relationships between traits (Bouxsein et al., 2010; Broeckhoven & du Pleissis, 2018). Limitations on time and money for μCT scanning also mean that specimen data are often collected haphazardly, constraining systematic analyses to one or few individuals per species. This trade-off between data accessibility and data quantity (and quality; Marcy et al., 2018) precludes the opportunity for more rigorous investigations of phenotypic diversity in time and space, as well as focused analyses of variation in a single taxon or locality. Common biodiversity metrics such as species identity, richness, and evenness are inferable from μCT data (e.g., Gray et al., 2017; Thorn et al., 2019), especially for cryptic taxa and species complexes with otherwise few observable differences (Chaplin et al., 2019; Melville et al., 2019; Caro et al., 2019). Therefore optimisation of the scanning process for high resolution 3D images of multiple specimens would not only contribute to our understanding of how biodiversity responds to global change, but also to the value of museum collections and researchers' abilities to access them digitally.

Here we outline steps for high throughput μCT scanning of small (< 2 cm) fossils, meant to facilitate advanced exploration of museum collections and allow researchers with limited access to specialised facilities the opportunity to maximize their investments. In contrast to other high-throughput μCT methods that have focused on automated phenotyping of laboratory strains (e.g., mice, Wong et al., 2014; rice, Wu et al., 2019; zebrafish, Ding et al., 2019), we concentrate on the practical arrangement of accessioned museum specimens so that each individual can be identified and labelled in the 3D volume, followed by long-term storage and archiving. We illustrate this method using vertebrate (lizard, frog, and mammal) fossils from the paleontological collections of Queensland Museum, Australia, as part of a larger effort to identify changes in morphology and species assemblages over deep time. We maximize the quantity of fossils per container to over 70 specimens to generate high quality 3D models for systematic analyses with minimal time, handling, and error. These steps should be applicable to any small dry objects of similar properties including geological material, plant tissues, and invertebrates, and wet specimens provided they can be mounted inside small capsules or other secure containers (e.g., Staedler et al., 2013; Keklikoglou et al., 2019).

Materials and methods

Preparation

The first step is the only time the user is required to handle fossil material directly, we therefore recommend the use of featherweight spring or feather light forceps and secondary

containment (see Figure 1 for an overview of packing material). Although specimens of varying size can be scanned together, it is preferable to organise fossils into batches of roughly similar material properties for X-ray optimization. Thin, unbuffered, neutral pH tissue is ideal for specimen packing and eventual long-term storage. Other required materials are small clear two-piece pharmaceutical capsules, paper and/or plastic drinking straws, archival paper and pen for labelling, a 50 ml plastic centrifuge tube with cap, and medium density polyethylene foam. Suggested suppliers and estimated costs of material per tube are listed in Table 1.

Packing procedure

Briefly, each specimen is wrapped in archival tissue and placed inside a capsule with its label, several of which are inserted lengthwise into a straw. Up to 14 standard paper straws cut to 9 cm in length fit inside a closed 50 ml Falcon tube, with each straw holding 6 size 4 capsules. For easier tracking of specimens, we recommend leaving one capsule empty in different positions along the length of some straws (see post-processing section below). Following this method, over 80 specimens < 1 cm long can be scanned in a single tube. This quantity can be doubled or tripled when 2 or 3 fossils (separated by tissue) are packed inside the same capsule, allowing a maximum of 252 specimens. However, scans with more than 3 specimens per capsule showed a high (≥ 50%) rate of movement during rotation, compared to those with fewer (Table 2). We therefore limit packing to 1-2 specimens per capsule, provided they can be distinguished from one another in relative size and/or shape. Specimens up to 2 cm long can be similarly packed inside size 00 capsules. Larger diameter paper or smoothie straws sliced lengthwise hold 3 size 00 capsules in a 50 ml tube (Fig. 1b), which can be scanned together with smaller straws as needed.

Labels for each specimen are written in Indian or archival ink on uncoated acid-free paper, providing a unique and durable identifier that will be matched in the 3D volume. Our labels followed a two-part system containing specimen ID (e.g., museum accession number) and a code for straw and capsule position. Using permanent marker, each straw is labelled with a letter (A, B, C…N for 14 straws) and each capsule is labelled with its straw's letter and a number from 1-6, denoting its position in the straw from top to bottom (Fig. 2a). This system can be amended to suit user needs, for example by including abbreviations for taxon if known and/or material (e.g., 'il' for ilium, 'max' for maxilla). These codes can also be extracted from the digital labels and used as variables in downstream analyses, e.g., in geomorph (Adams et al., 2019) or MorphoJ (Klingenberg, 2011). Record labels with capsule and straw positions, including any empty capsules as a marker, since these will be checked off later during unpacking.

Once labelling is complete, the specimens, labels, capsules and straws are aligned for packing. Each specimen is wrapped in a small envelope of Green's Lens tissue (Fig. 2b), and empty spaces in the capsule are filled with extra tissue so the specimen does not contact its walls. This creates more distance between adjacent samples, allowing easier separation (i.e. segmentation) in the 3D volume. The tissue also prevents movement during image acquisition (Table 2), which can lead to motion artefacts in the reconstruction like shadows or streaking. Finally, the label is inserted into the capsule with the ID facing out for long-term storage, and the capsules are loaded into their respective straws in the correct order. A thinner

cocktail straw can be used to gently push the capsules down without compressing ones below it (Fig. 2c).

To load the packed straws into the Falcon tube, first fill the conical tip with polyethylene or other firm material to create a flat surface. Insert the straws with position 1 towards this end, which will be facing up in the µCT machine. The flat surface of the cap on the other end can be fixed to a glass rod or dowel using a hot glue gun to elevate the tube from the machine's stage (Fig. 2d). This avoids including the metal clamp in the scan which would affect X-ray optimization, and centres the tube vertically and horizontally relative to the detector. Draw a diagram of the straw arrangement with the list of specimen labels, noting where paper or empty straws are used to separate them for easier identification (Fig. 2e,f). This material will be visible in reconstructed cross-sections, allowing one to match the 3D volume to the diagram. Finally, medium density foam can be cut and placed as filler around the straws and under the cap of the tube before closing. This foam is recommended over tissue or other supporting material as it acts as an effective shock absorber during rotation. Secure the tube onto the stage, making sure it can rotate freely without touching the X-ray source or detector.

X-ray parameters

Scan settings vary depending on the equipment, material size and properties, and desired results. Here we report parameters as optimised on a Phoenix nanotom m (GE Sensing & Inspection Technologies GmbH, Wunstorf, Germany) equipped with a 180 kV, 20 W high-power nanofocus X-ray tube and GE DXR detector (3072 x 2400 pixels). As with all microtomographic imaging, initial calibration of the detector is largely software-driven to reduce potential noise due to defective pixels or incident light. For all scans our instrument was fitted with a tungsten target, although molybdenum may be preferable for amber (Sutton et al., 2014). Fossils can be radiodense, in such cases reconstruction artefacts may occur when lower energy X-rays are attenuated at the surface (beam hardening), or when stronger X-rays hit the detector without passing through the object first (ring artefacts) (Sutton et al., 2014). A thin metal filter placed in front of the X-ray source can overcome these issues by removing the lowest energy photons, although other parameters like current, voltage, or exposure time should be modified to achieve appropriate contrast.

Ideally the number of images for reconstruction is equal to the maximum width of the scanned object in pixels × $\pi/2$ (du Plessis et al., 2017; Keklikoglou et al., 2019). For a sample optimized to fill the full width of our detector, this would result in nearly 5,000 projections at a resolution of 10.6 µm, accommodating a single 'row' of size 4 capsules. Such a data set would be massive in terms of scan time and storage (up to 70 GB before reconstruction), in addition to the computing power needed to render the 3D images. To improve the µCT process for smaller specimens without sacrificing image quality, we divided the Falcon tube into three segments by moving the position of the stage up or down between scans, while keeping all other settings identical. This produced separate volumes of equally high quality while avoiding the need to move the detector back and/or the tube forward to accommodate its length, thereby decreasing resolution. These volumes can be merged using Avizo (Thermo Fisher Scientific) or other dedicated software to recreate the entire tube in high resolution. However, for faster processing we aligned each segment to include two rows of size 4

capsules (or one row of size 00), so they could be separately visualised and labelled in the 3D volume if preferred.

For all reconstructions we followed the standard protocol of the Phoenix datos|x software (GE Sensing & Inspection Technologies GmbH, Wunstorf, Germany), which tests for object movement by comparing the first and last 2D projections. At high resolution, even minute movements can cause visible artefacts in the reconstructed images. Instead of correcting for movement of single specimens during the reconstruction by shifting the axis of rotation (which would in turn generate artefacts in the rest of the tube), we identified and labelled those specimens in post-processing so they could be rescannedf . Other settings applied during reconstruction were a 3×3 median filter and an ROI filter.

Computed tomography post-processing

Following reconstruction, digital labelling of the specimens is performed in 3D volume rendering software. Here we describe steps using VGStudioMax 3.1 (Volume Graphics, Heidelberg, Germany), although other options for free or commercial licenses are available (see Table 7 in Keklikoglou et al., 2019). To match the tube orientation to the diagram (Fig. 2f), the volume can be rotated in the 3D window or by using the registration tool in 2D. Straws can then be labelled digitally with the indicator tool or by creating a region of interest (ROI) to name each one by its letter (A, B, C… N). Similar-sized capsules should be aligned across the straws horizontally, making it easy to identify capsule positions in the 2D and 3D windows. For example, starting from the top (tip) of the tube in straw A, specimens should be ordered as A1, A2…A6, with capsules in the neighbouring straw B following the same order. Verifying the positions of empty capsules is another safeguard to ensure correct orientation. Using ROIs, the fossils can be segmented and renamed in the rendering software to match the specimen labels (e.g., museum accession number plus straw/capsule position). Colouring straws or capsule rows differently also helps to track specimen order. Any specimens with obvious artefacts can be marked with their labels followed by the word ‘REDO’, to be set aside during unpacking so they can be scanned again under improved conditions, i.e, repositioned in the capsule with better tissue support.

Unpacking and storage

Capsules are unpacked from the straws in the same manner as they were put in, by inserting a cocktail straw into one end and pushing it through (Fig. 2c). We recommend checking specimens off the list as they are being unpacked as a final test of correct labelling. These samples can be stored long-term inside the capsules since archival tissue and paper was used. Specimens for rescanning can be included in the next batch and labelled digitally with their ID, new straw and capsule position, and the word ‘REDONE’ for transparency. This process can be repeated as many times as necessary to achieve optimal quality scans for all material. Likewise, all labelled straws and Falcon tubes can be reused in subsequent scans, which will further ensure consistency in the packing and labelling process.

Results

Optimal settings for most of our fossils in terms of time, resolution and file size were three separate scans of the Falcon tube at 40 mm focus-to-object distance (FOD) and 225 mm focus-to-detector distance (FDD), using 40 kV, 300 µA, and 0.5 s exposure for 1400 images, with a frame average of 3 and image skip of 1. This configuration allowed us to decrease the width of the detector to 2,000 pixels, meaning that each X-ray image was 9.15 MB. The Y-axis of the stage was shifted down by 29 mm between scans to allow some overlap between segments (Fig. 3a). For each segment this resulted in a scan time of 47 minutes and 17.8 µm voxel size, with reconstructed volumes around 10 GB each (Fig. 3b). Stitching the separate segments together generated a single volume of equally high resolution (Fig. 3c), which was approximately 30 GB.

Cross-sectional µCT images revealed sharp contrast between the hydroxyapatite of the bone, dentine, and enamel against the clay and crystalline calcium carbonate-rich matrix, while offering precise details of specimen morphology as well as the dividing walls of the capsules, straws and paper (Fig. 3d-f). In few cases artefacts were observed in the reconstruction due to movement (Fig. 3g) or beam hardening (Fig. 3h). These specimens were labelled as 'REDO' in the 3D volume and set aside during unpacking to be rescanned, either with additional tissue in the capsule or using a filter, respectively. In earlier scans we observed some capsules in straws that had been slightly crushed by the one above it. These straws were packed using a solid dowel to push down the capsules, hence why we recommend using a cocktail straw instead.

Other examples of material scanned using our high throughput method are shown in Figure 4. Fossilized frog ilia and varanid osteoderms (bony deposits in the scales of some lizards) yielded excellent results following our protocol (Fig. 4ab), with hundreds of 3D models generated for minimal time, money and effort. We also applied our system to larger mammalian specimens, for example fossilized rodent jaws from the Middle Pleistocene Mt Etna fauna (Hocknull et al., 2007). This material is larger and denser than the herpetological samples, requiring slightly different parameters for µCT scanning. For larger/denser fossils, a 0.1 mm copper plate was secured under the collimator to reduce beam hardening and other artefacts, and X-ray voltage was increased to 50-80 kV. The resulting reconstructed images could be easily segmented using density-based approaches in VGStudioMax, like the region growing tool to separate teeth from bone (Fig. 4c).

Following digital labelling and unpacking, polygonal surface models of our specimens were extracted in VGStudioMax. Each model was exported from its ROI as an STL (sterolithography) file, retaining its original name. STL files capture the geometric shape of a 3D object using thousands of triangles or vertices to describe its surface (Fig. 4e). Such models, also known as meshes, are virtually interactive and can be manipulated, viewed, and measured using the open source software MeshLab (http://meshlab.sourceforge.net/). They are also small in terms of data storage, making them easy to distribute online and providing wider access to museum collections. These meshes can be scaled up for displays and educational programs, for example using 3D printing. Many of the fossils included in this project were excavated from cave deposits at Capricorn Caves in Rockhampton, Queensland. These scanned and 3D printed samples were later used to engage the public at an annual science communication event, the Capricorn Caves Fossil Open Day (Lawrence & Hocknull, 2019). There, palaeontologists referred to these enlarged 3D models to assist in the public

interpretation of microfossils, allowing children to interact with replicas of local animals from thousands of years in the past (Fig. 4f). In addition to public outreach, our future work will focus on analysing these data using a growing toolkit of bioinformatic approaches, including deep learning and AI, 3D landmark-based GM, and high-density point cloud conversion to compare fossil and living forms (Fig. 4f).

Conclusions

Current research on museum-based µCT data encompasses an extraordinary array of organisms and topics, including tetrapod origins (Long et al., 2006), echolocation in bats (Arbour et al., 2019) and whales (Park et al., 2016), limb reduction in lizards (Müller et al., 2011; Miralles et al., 2015), mammalian limb development (Weisbecker, 2011; Newton et al., 2018), primate neuroanatomy (Hublin et al., 2017; Beaudet & Gilissen, 2018), reproduction in insects (Wulff et al., 2015) and plants (Gee, 2013), paleoecology of Precambrian biota (Meyer et al., 2014), seafloor biomass estimation (Gooday et al., 2018) and amber inclusions (Dunlop et al., 2011, 2016), to name a few. Typically these studies have involved only few specimens, due to the difficulties of capturing high resolution 3D phenotypic data for large sample sizes.

Here we demonstrate how simple, inexpensive equipment like drinking straws and pharmaceutical capsules can be modified for high throughput µCT scanning of dozens of fossils in a single tube, providing large-scale paleontological data sets for macroevolutionary analyses. To date we have scanned over 1,000 accessioned museum specimens following this technique, including 360 frogs, 630 lizards, and over a dozen mammals. These data will contribute to ongoing efforts to identify evolutionary responses to climate change in Australia's fossil record, where reptiles and amphibians constitute half of the terrestrial vertebrate diversity, and where increasing aridity has transformed large parts of the continent. These methods can also be adapted for other (non-biological) objects, by creating custom-made holders and stages, and seeking µCT scanners with differing capacities. At the same time we note that fossils can be difficult to scan, being highly variable in shape, composition, and density. Thus while µCT is a powerful tool for most small specimens, in some cases other non-destructive techniques such as magnetic resonance imaging (MRI), synchrotron, and confocal microscopy may be more appropriate.

Acknowledgements

This work was supported by an Australian Research Council DECRA (DE180100629) to CAH, with scans performed through the Melbourne TrACEES platform. Danielle Measday, Conservator of Natural Sciences at Museums Victoria, advised on and provided archival papers for testing. We thank Kristen Spring, Rochelle Lawrence, Joanne Wilkinson, and Jonathan Cramb, along with many volunteers at the Queensland Museum, for their assistance in generating the large quantity of specimens made available for this project.

Authors' contributions

CAH and SH conceived the project; SH selected specimens for µCT scanning; CAH, RA, and JRB designed the methodology; JRB operated the µCT machine; CAH and RA collected

370 and analysed the data and led manuscript writing. All authors contributed to initial drafts and
371 gave final approval for publication.
372
373 **References**
374
375 Adams, D., Collyer, M., & Kaliontzopoulou, A. (2019). Geomorph: Software for geometric
376 morphometric analyses. R package version 3.1.0. https://cran.r-
377 project.org/package=geomorph.
378 Akkari, N., Ganske. A.-S., Komerički, A., & Metscher, B. (2018). New avatars for
379 Myriapods: complete 3D morphology of type specimens transcends conventional
380 species description (Myriapoda, Chilopoda). PLoS ONE, 13, e0200158.
381 Arbour, J. H., Curtis, A. A., & Santana, S. E. (2019). Signatures of echolocation and dietary
382 ecology in the adaptive evolution of skull shape in bats. Nature Communications, 10,
383 2036. doi: 10.1038/s41467-019-09951-y.
384 Beaudet, A., & Gilissen, E. (2018). Fossil primate endocasts: perspectives from advanced
385 imaging techniques. In E. Bruner, N. Ogihara, & H. Tanabe (Eds.), *Digital Endocasts:*
386 *from Skulls to Brains* (pp. 47-58), Nagoya, Springer.
387 Bouxsein, M. L., Boyd, S. K., Christiansen, B. A., Guldberg, R. E., Jepsen, K. J., Müller, R.
388 (2010). Guidelines for assessment of bone microstructure in rodents using micro –
389 computed tomography. Journal of Bone and Mineral Research, 25, 1468-1486.
390 Broeckhoven, C., & du Pleissis, A. (2018). X-ray microtomography in herpetological
391 research: a review. Amphibia-Reptilia, 39, 377-401.
392 Caro, A., Gomez-Moliner, B. J., & Madeira, M. J. (2019). Integrating multilocus DNA data
393 and 3D geometric morphometrics to elucidate species boundaries in the case of
394 Pyrenaearia (Pulmonata: Hygromiidae). Molecular Phylogenetics and Evolution,
395 132, 194–206.
396 Chaplin, K., Sumner, J., Hipsley, C. A., & Melville J. (2019). An integrative approach using
397 phylogenomics and high-resolution x-ray computed tomography for species
398 delimitation in cryptic taxa. Systematic Biology, syz048.
399 Chira, A. M., Cooney, C. R., Bright, J. A., Capp, E. J. R., Hughes, E. C., Moody C. J. A.,
400 Nouri, L. O., Varley, Z. K., & Thomas G. H. (2018). Correlates of rate heterogeneity
401 in avian ecomorphological traits. Ecology Letters, 21, 1505-1514. doi:
402 10.1111/ele.13131.
403 Ding, Y., Vanselow, D. J., Yakovlev, M. A., Katz, S. R., Lin, A. Y., Clark, D. P., Vargas, P.,
404 Xin, X., Copper, J. E., Canfield, V. A., Ang, K. C., Wang, Y., Xiao, X., De Carlo, F.,
405 van Rossum, D. B., La Riviere, P., & Cheng K. C. (2019). Computational 3D
406 histological phenotyping of whole zebrafish by X-ray histotomography. Elife 8,
407 e44898. doi: 10.7554/eLife.44898.
408 Dunlop, J. A., Penney, D., Dalüge N., Jäger, P., McNeil, A., Bradley, R. S., Withers, P. J., &
409 Preziosi, R. F. (2011). Computed tomography recovers data from historical amber: an
410 example from huntsman spiders. Naturwissenschaften 98, 519-527.
411 Dunlop, J. A., Apanaskevich, D. A., Lehmann, J., Hoffmann, R., Fusseis, F., Ehlke, M.,
412 Zachow, S., & Xiao, X. (2016). Microtomography of the Baltic amber tick *Ixodes*

succineus reveals affinities with the modern Asian disease vector Ixodes ovatus. BMC Evolutionary Biology, 16, 203.

Elliott, J. C., & Dover, S. D. (1982). X-ray microtomography. Journal of Microscopy, 126, 211-213.

Elliott, J. C., & Dover, S. D. (1985). X-ray microscopy using computerized axial tomography. Journal of Microscopy, 138, 329-331.

Faulwetter, S., Vasileiadou, A., Kouratoras, M., Dailianis, T., & Arvanitidis, C. (2013). Micro-computed tomography: Introducing new dimensions to taxonomy. ZooKeys, 263, 1–45.

Faulwetter, S., Dailianis, T., Vasileiadou, K., Kouratoras, M., & Arvanitidis, C. (2014). Can micro-CT become an essential tool for the 21st century taxonomist? An evaluation using marine polychaetes. Microscopy and Analysis, 28, s9-s11.

Fontaine ,B., Perrard, A., & Bouchet, P. (2012). 21 years of shelf life between discovery and description of new species. Current Biology, 22, R943.

Gee, C. T. (2013). Applying microCT and 3D visualization to Jurassic silicified conifer seed cones: a virtual advantage over thin-sectioning. Applications in Plant Sciences, 1, 1300039.

Gooday, A. J., Sykes, D., Goral, T., Zubkov, M. V., & Glover, A.G. (2018). Micro-CT 3D imaging reveals the internal structure of three abyssal xenophyophore species (Protista, Foraminifera) from the eastern equatorial Pacific Ocean. Scientific Reports, 8, 12103.

Gray, J. A., McDowell, M. C., Hutchinson, M. N., & Jones, M. E. (2017). Geometric morphometrics provides an alternative approach for interpreting the affinity of fossil lizard jaws. Journal of Herpetology, 51, 375-382.

Hocknull, S. A., Zhao, J. X., Feng, Y. X., & Webb, G. E. (2007). Responses of middle Pleistocene rainforest vertebrates to climate change in Australia. Earth and Planetary Science Letters, 264, 317-331.

Hipsley, C. A., & Sherratt ,E. (2019). Psychology, not technology, is our biggest challenge to open digital morphology data. Scientific Data, 6, 41.

Hublin, J. J., Ben-Ncer, A., Bailey, S. E., Freidline, S. E., Neubauer, S., Skinner, M. M., Bergmann, I., Le Cabec, A., Benazzi, S., Harvati, K., & Gunz, P. (2017). New fossils from Jebel Irhoud, Morocco and the pan-African origin of Homo sapiens. Nature, 546, 289-292.

Keklikoglou, K., Faulwetter , S., Chatzinikolaou, E., Wils, P., Brecko, J., Kvaček, J., Metscher, B., & Arvanitidis, C. (2019). Micro-computed tomography for natural history specimens: a handbook of best practice protocols. European Journal of Taxonomy 522, 1-55.

Ketcham, R. A. (2005). Computational methods for quantitative analysis of three-dimensional features in geological specimens. Geosphere, 1, 32-41.

Klingenberg, C. P. (2011). MorphoJ: an integrated software package for geometric morphometrics. Molecular Ecology Resources, 11, 353-357.

Lawrence, R. A., & Hocknull, S. (2019). Engaging the public with small vertebrate fossils and utilizing citizen science to maximise scientific discovery at Capricorn Caves,

Central Eastern Queensland, Australia. Journal of Vertebrate Paleontology, Program and Abstracts, 139.

Long, J. A., Young, G. C., Holland, T., Senden, T. J., & Fitzgerald, E. M. (2006). An exceptional Devonian fish from Australia sheds light on tetrapod origins. Nature, 444, 199-202.

Marcy, A. E., Fruciano, C., Phillips, M. J., Mardon, K., & Weisbecker, V. (2018). Low resolution scans can provide a sufficiently accurate, cost- and time-effective alternative to high resolution scans for 3D shape analyses. PeerJ, 6, e5032. doi: 10.7717/peerj.5032

Melville, J., Chaplin, K., Hipsley, C. A., Sarre, S., Sumner, J., & Hutchinson, M. (2019). Integrating phylogeography and high-resolution x-ray CT reveals five new cryptic species and multiple hybrid zones among Australian earless dragons. Royal Society Open Science, 6. http://doi.org/10.1098/rsos.191166.

Meyer, M., Elliott, D., Wood, A. D., Polys, N. F., Colbert, M., Maisano, J. A., Vickers-Rich, P., Hall, M., Hoffman, K. H., Schneider, G., & Xiao, S. (2014). Three-dimensional microCT analysis of the Ediacara fossil Pteridinium simplex sheds new light on its ecology and phylogenetic affinity: Precambrian Research, 249, 79-87.

Miralles, A., Hipsley, C. A., Erens, J., Gehara, M., Rakotoarison, A., Glaw, F., Müller, J., & Vences, M. (2015). Distinct patterns of desynchronized limb regression in Malagasy scincine lizards (Squamata, Scincidae). PLoS ONE 10(6): e0126074.

Müller, J., Hipsley, C. A., Head, J. J., Kardjilov, N., Hilger, A., Wuttke, M., & Reisz, R. R. (2011). Eocene lizard from Germany reveals amphisbaenian origins. Nature, 473, 364–367.

Newton, A. H., Spoutil, F., Prochazka, J., Black, J. R., Medlock, K., Paddle, R. N., Knitlova, M., Hipsley, C. A., & Pask, A. J. (2018). Letting the 'cat' out of the bag: pouch young development of the extinct Tasmanian tiger revealed by X-ray computed tomography. Royal Society Open Science 5,171914. http://dx.doi.org/10.1098/rsos.171914

Page, L. M., MacFadden, B. J., Fortes, J. A., Soltis, P. S., & Riccardi G. (2015). Digitization of biodiversity collections reveals biggest data on biodiversity. BioScience, 65, 841–842.

Park, T., Fitzgerald, E. M., & Evans, A. R. (2016). Ultrasonic hearing and echolocation in the earliest toothed whales. Biology Letters, 12, 20160060. doi: 10.1098/rsbl.2016.0060.

Sato, T., Ikeda, O., Yamakoshi, Y., & Tsubouchi, M. (1981). X-ray tomography for microstructural objects. Applied Optics, 20, 3880-3883.

Percival, C. J., Devine, J., Darwin, B. C., Liu, W., van Eede, M., Henkelman, R. M., &Hallgrimsson, B. (2019). The effect of automated landmark identification on morphometric analyses. Journal of Anatomy, 234, 917-935.

Schindelin, J., Arganda-Carreras, I., Frise, E., Kaynig, V., Longair, M., Pietzsch, T., Preibisch, S., Rueden, C., Saalfeld, S., Schmid, B., Tinevez, J. Y., White, D.J., Hartenstein, V., Eliceiri, K., Tomancak, P., & Cardona, A. (2012). Fiji: an open-source platform for biological-image analysis. Nature Methods, 9, 676-682.

Sherratt, E., Alejandrino, A., Kraemer, A. C., Serb, J. M., & Adams, D. C. (2016). Trends in the sand: directional evolution in the shell shape of recessing scallops (Bivalvia: Pectinidae). Evolution, 70, 2061-73. doi: 10.1111/evo.12995.

Sherratt, E., Serb, J. M., & Adams, D. C. (2017). Rates of morphological evolution, asymmetry and morphological integration of shell shape in scallops. BMC Evolutionary Biology, 17, 248.

Simon, M. N., Machado, F. A., & Marroig, G. (2016). High evolutionary constraints limited adaptive responses to past climate changes in toad skulls. Proceedings of the Royal Society B, 283, 20161783. http://doi.org/10.1098/rspb.2016.1783.

Staedler, Y. M., Masson, D., & Schönenberger, J. (2013). Plant tissues in 3D via X-ray tomography: simple contrasting methods allow high resolution imaging. PLoS ONE, 8, e75295.

Sutton, M., Rahman, I., & Garwood, R. (2014). Techniques for Virtual Palaeontology. New York, John Wiley & Sons,.

Thorn, K. M., Hutchinson, M. N. Archer, M., & Lee, M. S. Y. (2019). A new scincid lizard from the Miocene of northern Australia, and the evolutionary history of social skinks (Scincidae: Egerniinae). Journal of Vertebrate Paleontology, 39, 1. doi: 10.1080/02724634.2019.1577873

Watanabe, A., Fabre, A. C., Felice, R. N., Maisano, J. A., Müller, J., Herrel, A., & Goswami, A. (2019). Ecomorphological diversification in squamates from conserved pattern of cranial integration. Proceedings of the National Academy of Sciences, 116, 14688-14697.

Weisbecker, V. (2011). Monotreme ossification sequences and the riddle of mammalian skeletal development. Evolution, 65, 1323-1335. doi: 10.1111/j.1558-5646.2011.01234.x.

Wong, M. D., Maezawa, Y., Lerch, J. P., & Henkelman, R. M. (2014). Automated pipeline for anatomical phenotyping of mouse embryos using micro-CT. Development, 141, 2533–2541.

Wu, D., Guo, Z., Ye, J., Feng, H., Liu, J., Chen, G., Zheng, J., Yan, D., Yang, X., Xiong, X., Liu, Q., Niu, Z., Gay, A. P., Doonan, J. H., Xiong, L., & Yang, W. (2019). Combining high-throughput micro-CT-RGB phenotyping and genome-wide association study to dissect the genetic architecture of tiller growth in rice. Journal of Experimental Botany, 70, 545–561.

Wulff ,N. C., Lehmann, A. W., Hipsley, C. A., Lehmann, G. U. C. (2015). Copulatory courtship by bushcricket genital titillators revealed by functional morphology, µCT scanning for 3D reconstruction and female sense structures. Arthropod Structure and Development 44, 388- 397.

Tables

Table 1. Estimated costs in USD for packing material to µCT scan 70 small (< 1 cm long) fossils in a 50 ml cylinder. Note that many items (e.g., Falcon tube, straws, forceps, foam, litter tray, pen) can be reused multiple times, further bringing down the cost for subsequent scans.

Item	Total cost per scan (USD)
Centrifuge Falcon Tube 50 mL polypropylene (PP), conical bottom with screw cap[1]	0.44
Hard 2-piece clear gelatine capsules, size 4 (volume 0.23 ml)[2*]	1.43
Standard paper straw (6 x 135 mm)[3]	0.09
Green's Lens Tissue, un-buffered TIS-L Soft, acid-free, long fibred 9gsm repair/wrapping tissue (609 x 914 mm)[4]	0.52
Feather Forcep Sharp E122S, 0.23 mm gauge thick[5]	3.33
Ethafoam 220, medium density, non-cross linked Polyethylene (PE) closed cell foam (2400 x1200 mm)[6]	0.68
Litter tray[7]	2.72
Label paper, ¼ sheet [8]	8.72
Archival pen [9]	4.04
TOTAL	21.97

Suppliers: [1]https://corning.com.au; [2]https://gelcapsules.com.au; [3]https://www.greenpack.com.au; [4]http://www.archivalsurvival.com.au; [5]http://www.entosupplies.com.au; [6]https://www.foamsales.com.au; [7]https://www.kmart.com.au; [8]https://www.talasonline.com; [9]https://www.newtownartsupplies.com.au/

*Clear 2-piece vegetable capsules are also available, although we did not test their performance in µCT scans.

553 **Table 2.** Estimated movement among 408 fossils μCT scanned using various packing
554 materials to secure the specimen inside the capsule.
555

Packing material	Number of specimens per capsule (size 4) that moved during scanning			Archival?	Comments
	1-2	3	> 3		
Green's Lens[1]	0/100 (0%)	2/39 (5.1%)	25/50 (50%)	Yes	Ideal consistency
Kim Tech wipes[2]	0/100 (0%)	4/39 (10.3%)	27/50 (54%)	No	100% fibre, not acid free
Ethafoam 220[3]	10/10 (100%)	10/10 (100%)	10/10 (100%)	No	Slippery and hard
Tyvek[4]	-	-	-	Yes	Not tested, too waxy
Renaissance[5]	-	-	-	Yes	Not tested, too rigid

556 Suppliers: [1]http://www.archivalsurvival.com.au; [2]https://www.kcprofessional.com.au;
557 [3]https://www.foamsales.com.au; [4]http://www.dupont.com.au;
558 [5]http://www.lightimpressionsdirect.com
559

Figures

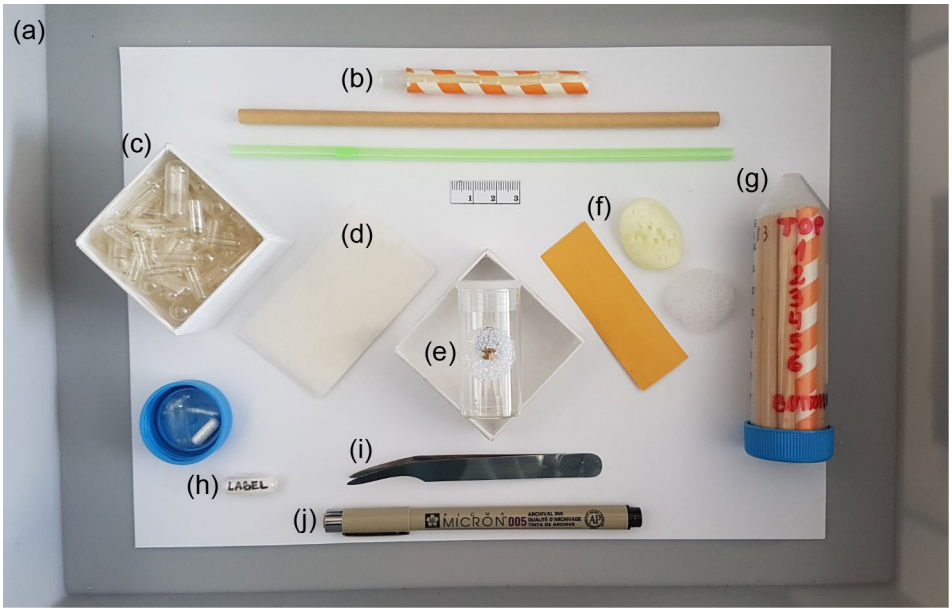

Figure 1 Equipment for dense fossil packing prior to µCT scanning: (a) litter tray, (b) paper and/or plastic straws, (c) clear two-piece pharmaceutical capsules, (d) archival tissue, (e) dry fossil specimen, (f) supporting material (paper, foam), (g) centrifuge tube with cap, (h) archival paper for labels shown inside a size 4 capsule, (i) forceps, (j) archival pen. Estimated costs and material suppliers are listed in Table 1.

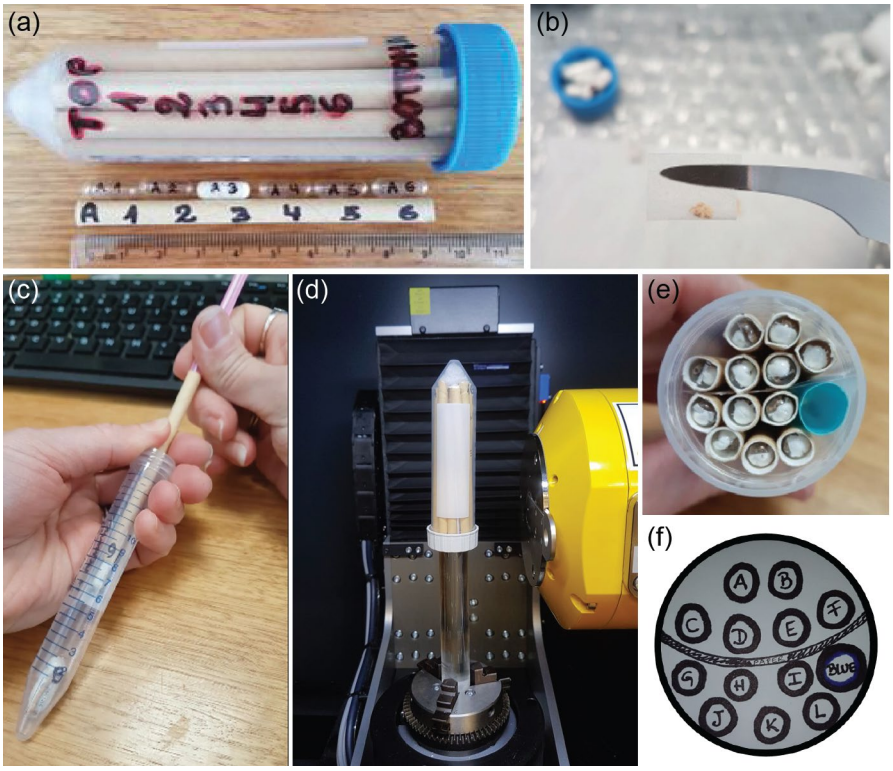

Figure 2 Specimen labelling and packing: (a) 50 ml Falcon tube with a labelled straw and capsules, (b) a single fossil wrapped in Green's Lens tissue to reduce movement inside the capsule, (c) loading capsules into the paper straw using a thinner cocktail straw to gently push them down, (d) a packed 50 ml Falcon tube mounted on a glass rod inside the µCT machine, note that the cap-side is facing down (e) the packed tube from above, and (f) the diagram of straw arrangements in (e), noting the position of a larger blue straw and paper used as a divider.

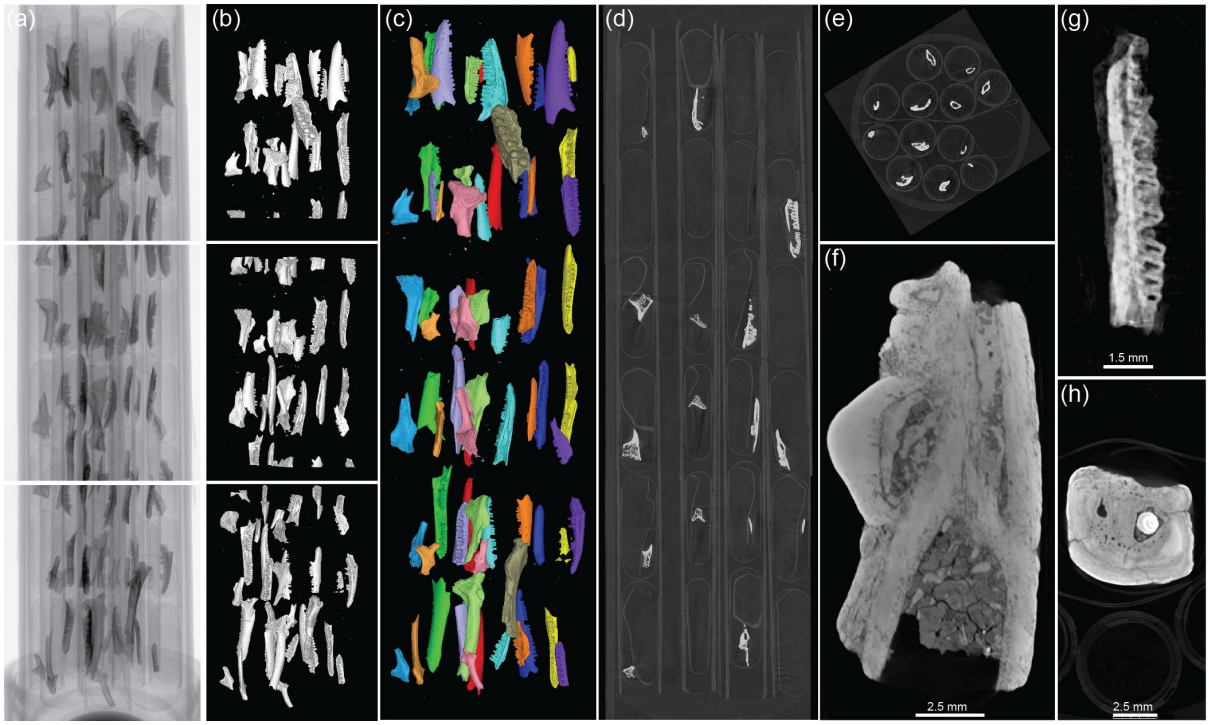

Figure 3 High throughput µCT results: (a) the first X-ray image from each scanned segment of the 50 ml tube from top (tip) to bottom (cap), containing 72 frog and lizard specimens. (b) 3D renderings of the individual segments in the same positions, at 17.8 µm voxel size , (c) the stitched 3D volume at the same resolution, with fossils colour-coded by straw, (d) reconstructed cross-section of the same tube in side and (e) top views, (f) cross-section of an agamid lizard jaw showing sharp contrast between the matrix, bone, and teeth, (g) cross-section of a skink mandible with a shadow motion artefact, (h) an example of beam hardening caused by dense infilling matrix material.

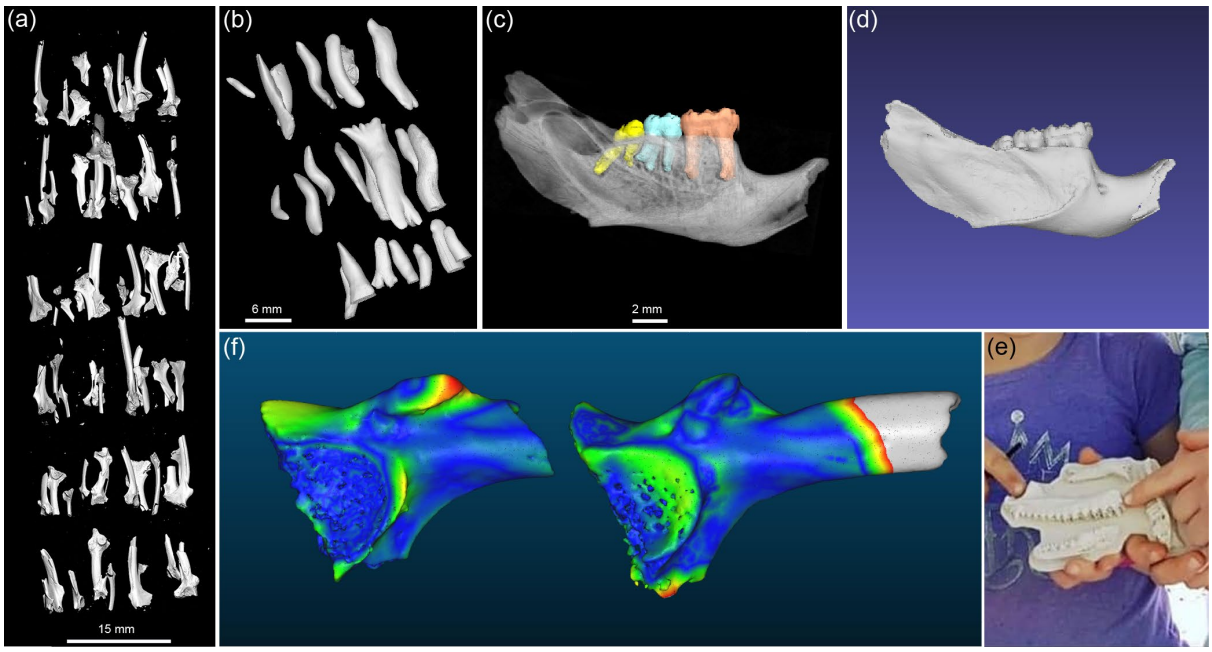

Figure 4 Scanned fossil material and its applications: (a) 3D rendering of 73 fossil frog ilia scanned in a single tube, (b) a subsample of varanid osteoderms, (c) mandible of the rainforest rodent *Pogonomys* from the Riversleigh World Heritage site with molars colour coded and jaw bone rendered semi-transparent, (d) surface mesh of the same specimen composed of 109,213 vertices (file size 10.5 MB), (e) children holding a 3D print of enlarged fossil skink jaws at Capricorn Caves Fossil Open Day 2019, (f) point cloud comparison of fossil tree frog (Hylidae) ilia found at 10-20 cm depth (left) in Capricorn Caves and 40-50 cm depth (right), representing a time difference of 2-3,000 years. Warmer colours denote regions with greater shape differences.